



Factors influencing thermal solidification of bent-core trimers

Cite as: J. Chem. Phys. 151, 134501 (2019); <https://doi.org/10.1063/1.5121163>

Submitted: 24 July 2019 . Accepted: 13 September 2019 . Published Online: 01 October 2019

Elvin D. Salcedo , Hong T. Nguyen, and Robert S. Hoy 



View Online



Export Citation



CrossMark

Lock-in Amplifiers up to 600 MHz

starting at

\$6,210



 Zurich
Instruments

Watch the Video 

AIP
Publishing

Factors influencing thermal solidification of bent-core trimers

Cite as: J. Chem. Phys. 151, 134501 (2019); doi: 10.1063/1.5121163

Submitted: 24 July 2019 • Accepted: 13 September 2019 •

Published Online: 1 October 2019



View Online



Export Citation



CrossMark

Elvin D. Salcedo,¹  Hong T. Nguyen,² and Robert S. Hoy^{1,a)} 

AFFILIATIONS

¹Department of Physics, University of South Florida, Tampa, Florida 33620, USA

²Department of Materials Science and Engineering, University of Texas at Dallas, Richardson, Texas 75080, USA

Note: This paper is part of the JCP Emerging Investigators Special Collection.

^{a)}rshoy@usf.edu

ABSTRACT

Bent-core trimers are a simple model system for which the competition between crystallization and glass-formation can be tuned by varying a single parameter: the bond angle θ_0 . Using molecular dynamics simulations, we examine how varying θ_0 affects their thermal solidification. By examining trends with θ_0 , comparing these to the trends in trimers' jamming phenomenology, and then focusing on the six θ_0 that are commensurate with close-packed crystalline order, we obtain three key results: (i) the increase in trimers' solidification temperature $T_s(\theta_0)$ as they straighten (as $\theta_0 \rightarrow 0^\circ$) is driven by the same gradual loss of *effective* configurational freedom that drives athermal trimers' decreasing $\phi_f(\theta_0)$ [where $\phi_f(\theta_0)$ is the packing fraction at jamming]; (ii) θ_0 that allow formation of both FCC and HCP order crystallize, while θ_0 that only allow formation of HCP order glass-form; and (iii) local cluster-level structure at temperatures slightly *above* $T_s(\theta_0)$ is highly predictive of whether trimers will crystallize or glass-form.

Published under license by AIP Publishing. <https://doi.org/10.1063/1.5121163>

I. INTRODUCTION

Bent-core trimers are a simple model for many small organic molecules whose bulk liquids exhibit both crystallization and glass-formation in experiments.^{1–4} Their shape can be characterized using three dimensionless parameters (Fig. 1): the bond angle θ_0 , the ratio \tilde{r} of the end-monomer radius to the center-monomer radius, and the ratio R of the bond length to the center-monomer diameter. It is well known that the properties of systems composed of such molecules depend strongly on all three of these parameters. For example, the three terphenyl isomers, which can be modeled as trimers with the same \tilde{r} and R but different θ_0 , form very differently structured bulk solids under the same preparation protocol.¹ Analogous θ_0 -dependent differences occur between the three xylene isomers.² Two more classes of small molecules, the diphenyl-cycloalkenes and cyclic stilbenes, which can each be modeled as having the same θ_0 but different \tilde{r} and R , show similarly complex and poorly understood dependence of crystallizability on molecular shape.^{3,4}

One of the reasons why our understanding of such phenomena and hence our ability to engineer crystallizability/glass-formability

at the molecular level remains very limited is that only a few theoretical studies have isolated the role played by molecular shape using simple models. Reference 5 reported the densest packings of 2D $R = 1/2$ trimers as a function of \tilde{r} and θ_0 . References 6–8 examined the thermal solidification of Lewis-Wahnstrom-like models ($R = 2^{-1/6}$, $\tilde{r} = 1$, $\theta_0 = 105^\circ$) and reported several non-trivial effects of trimeric structure, e.g., that its enhancement of the interfacial energy between crystalline and liquid phases promotes glass-formation. The tangent-sphere ($\tilde{r} = R = 1$) case shown in Fig. 1(b) is of considerable interest because it allows straightforward connection to results obtained for monomers—and hence isolation of the role played by the bond and angular constraints—while remaining a reasonable minimal model for trimeric molecules. References 10 and 11 reported the densest packings of 2D and 3D trimers and contrasted them to the jammed packings they form under dynamic athermal compression. Reference 12 examined how the dynamics of supercooled trimer liquids vary with θ_0 .

In this paper, we examine the thermal solidification of bent-core tangent-sphere Lennard-Jones trimers as a function of their bond angle θ_0 using molecular dynamics simulations. We obtain

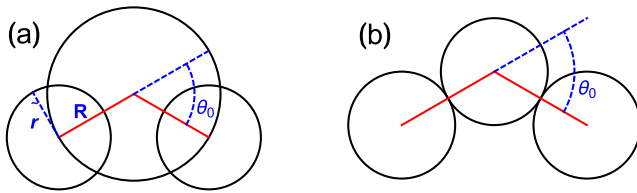


FIG. 1. Rigid bent-core trimers with bond angle θ_0 . Panel (a) shows the general geometry with unspecified (\bar{r}, R) . Here, we study the $\bar{r} = R = 1$ case shown in panel (b).

three key results: (i) the sharply increasing solidification temperature $T_s(\theta_0)$ for $\theta_0 \lesssim 20^\circ$ is driven by the same gradual loss of *effective* configurational freedom that drives athermal trimers' decreasing $\phi_j(\theta_0)$;¹¹ (ii) θ_0 that allow formation of both FCC and HCP order crystallize, while θ_0 that only allow formation of HCP order glass-form; (iii) measurements of local cluster-level structure via characteristic crystallographic element (CCE) and topological cluster classification (TCC) analyses^{13,14} are as predictive of whether trimers will crystallize or glass-form as they are for monomeric systems.

II. MODEL AND METHODS

A. Molecular dynamics simulations

Each simulated trimer contains three monomers of mass m . These trimers are rigid; their bond lengths and angles are held fixed by holonomic constraints. Monomers belonging to different trimers interact via the truncated and shifted Lennard-Jones potential,

$$U_{LJ}(r) = \epsilon \left[\left(\frac{\sigma}{r} \right)^{12} - \left(\frac{\sigma}{r_c} \right)^{12} - 2 \left(\left(\frac{\sigma}{r} \right)^6 - \left(\frac{\sigma}{r_c} \right)^6 \right) \right], \quad (1)$$

where ϵ is the energy scale of the pair interactions, σ is the monomer diameter, and $r_c = 2^{7/6}\sigma$ is the cutoff radius.

The Lewis-Wahnstrom model⁹ is a good glass-former largely because its equilibrium backbone bond length ℓ_0 is incommensurable with its equilibrium nearest neighbor distance for nonbonded neighbors r_0 ; specifically, it has $\ell_0 = \sigma$ and $r_0 = 2^{1/6}\sigma$. In contrast, the current model makes these lengths commensurable ($\ell_0 = r_0 = \sigma$). Any frustration against crystallization is driven primarily by the bond angle θ_0 .^{15,16} Six θ_0 are commensurable with 3D close-packing: 0° , $\cos^{-1}(5/6) \approx 33.5^\circ$, 60° , $\cos^{-1}(1/3) \approx 70.5^\circ$, 90° , and 120° .¹¹ All of these θ_0 allow formation of HCP crystals, whereas only 0° , 60° , 90° , and 120° allow formation of FCC crystals. We will argue below that this distinction is critical.

Initial states are generated by placing $n_{tri} = 1333$ trimers randomly within a cubic cell of volume $V_0 = \pi n_{tri} \sigma^3$. Periodic boundary conditions are applied along all three directions and Newton's equations of motion are integrated with a time step $\delta t = 0.005\tau$, where the unit of time is $\tau = \sqrt{m\sigma^2/\epsilon}$. Fixed covalent bond lengths and bond angles are maintained using a standard method.¹⁷ Systems are equilibrated at temperature $k_B T = \epsilon$ and pressure $P = 0$ until the intertrimer structure has converged, then cooled to $T = 0$ at a rate

$\dot{T} = -10^{-6}\epsilon/(k_B\tau)$ while maintaining zero pressure. All MD simulations are performed using LAMMPS.¹⁸

During the cooling runs, we monitor the cell volume $V(T)$ and, hence, the monomer number density $\rho(T) = 3n_{tri}/V(T)$ and packing fraction $\phi(T) = \pi\rho(T)\sigma^3/6$.¹⁹ We then identify the solidification temperature T_s of each system using one of the two methods. For systems exhibiting crystallization, we simply locate the center of the first-order-transitionlike jump in $\phi(T)$ as T decreases. For systems exhibiting glass-formation, we identify T_s as the intersection points of linear fits to the high- and low- T portions of their $\phi(T)$ curves. Consistent with our focus on trimers' solidification under *dynamic* cooling, these $T_s(\theta_0)$ are below the equilibrium solid-liquid transition temperatures $T_{melt}(\theta_0): T_s(\theta_0) = T_{melt}(\theta_0) - \Delta T(\theta_0, \dot{T})$, where ΔT increases with $|\dot{T}|$ and with glass-formability. The cooling rate employed here approaches the lowest rate that is currently computationally feasible for the n_{tri} and number of different θ_0 we study. When mapped to real units using the Lewis-Wahnstrom parameter values for *ortho*-terphenyl (OTP) ($m = 1.27 \times 10^{-25}$ kg, $\sigma = 4.83 \times 10^{-9}$ m, and $\epsilon = 8.28 \times 10^{-21}$ J⁹), $|\dot{T}| = 10^{-6}\epsilon/(k_B\tau) = 5.27 \times 10^4$ K/s. Although this rate is quite large, it is well within the range of $|\dot{T}|$ achievable in experiments²¹ and is low enough that $\Delta T(\theta_0)$ is small for our best crystal-formers. A further discussion of cooling-rate effects is given in the [Appendix](#).

B. Measures of local order

We characterize systems' local structure using the characteristic crystallographic element (CCE)¹³ and topological cluster classification (TCC)¹⁴ methods. Recent studies employing CCE^{22–24} or TCC^{25–29} analyses have led to much progress in our understanding of thermal solidification. These studies have found that the presence of energetically stable amorphous clusters in a system's liquid state (at temperatures slightly above its T_{melt}) strongly promotes glass-formation. Long-lived clusters that are fivefold-symmetric and/or are subsets of icosahedra are particularly effective glass-promoters.^{22,23,27,28}

CCE employs descriptors known as “norms” that quantify the orientational and radial similarities of a given monomer's local environment to those of various reference structures such as HCP and FCC crystals.¹³ These norms are built around sets of point symmetry groups that uniquely characterize the reference structure. Criteria based on these norms are applied to determine whether the monomer can be associated with structure X. Here, we identify monomers as FCC-like, HCP-like, or fivefold-like if their respective norms n_X (where $X = \text{FCC, HCP, or } 5f$) are less than 0.21. Monomers that satisfy none of these conditions are classified as “other”; these typically possess locally amorphous order. The relevant mathematical formulas and the algorithmic implementation are described in Ref. 13.

TCC is similar in spirit to CCE, but identifies differently structured clusters by their differing bond topology. Here, we employ TCC to track how the populations of various microstructural motifs within our systems vary with θ_0 and T , using the same procedures detailed in Ref. 14. We focus on the four cluster types shown in Fig. 2. 6A is the octahedron, a common motif in close-packed crystals. 6Z, a polytetrahedral structure, has higher energy but also much higher entropy than 6A³⁰ and is a common motif in glassy and jammed systems.³¹ 9B is a partial icosahedron; recall that icosahedral order

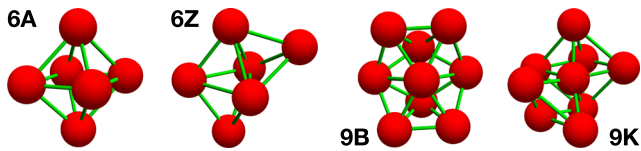


FIG. 2. The four clusters of primary interest for our TCC analyses. Red spheres correspond to monomer positions, while green lines indicate neighboring; the sphere diameter is reduced here for clarity. We will show that the θ_0 - and T -dependencies of these clusters' formation propensities are strongly coupled.

has long been known to promote glass-formation.³² Finally, 9K is a subset of the HCP lattice.

During the cooling runs, we monitor the fractions $f_X(T)$ of particles identified as X-like (for CCE analyses) or belonging to at least one cluster of type X (for TCC analyses). We will show below that θ_0 -dependent differences in how these quantities evolve with decreasing T predict whether a given system will crystallize or glass-form.

III. RESULTS

A. Macroscopic

Figure 3 summarizes the most basic features of bent-core trimers' response to slow thermal cooling. Panel (a) shows the packing fraction $\phi(T)$ for the six values of θ_0 that are commensurable with 3D close-packing and contrasts these to results for monomers. Three features are immediately apparent. First, some θ_0 produce sharp, first-order-transitionlike jumps in $\phi(T)$ that indicate rapid crystallization, while others produce typical glassy behavior where a smooth crossover regime centered at $T \simeq T_g(\theta_0)$ connects roughly linear behavior at high and low T . It is noteworthy that some θ_0 that are commensurable with the formation of close-packed crystals glass-form even at the low cooling rate ($|\dot{T}| = 10^{-6}/\tau$) employed here. Second, even for those systems that do crystallize, the sharpness of the transition depends strongly on θ_0 ; systems with sharper transitions (e.g., $\theta_0 = 120^\circ$) have faster crystallization kinetics. Third, trimers always solidify at higher temperatures and lower densities than their monomeric counterparts.

As shown in Fig. 3(b), trimers' solidification temperatures remain relatively constant as θ_0 decreases from 120° to $\sim 20^\circ$, then increase rapidly as $\theta_0 \rightarrow 0^\circ$. This trend presumably results from the loss of *effective* configurational freedom as trimers approach linearity. Specifically, the middle monomer in a bent trimer can relax away from obstacles by rotating about the line connecting the end monomers even if the end monomers are held fixed, whereas the middle monomer in a straight trimer cannot. The same decrease in effective configurational freedom appears to drive the decreasing ϕ_I in athermal bent-core trimers¹¹ as well as the increasing fragility of bidisperse bent-core trimer liquids¹² as $\theta_0 \rightarrow 0^\circ$. See the Appendix for a discussion of how this decrease might influence trimers' θ_0 -dependent liquid-state dynamics.

Figure 3(c) shows the packing fractions $\phi(T)$ for all θ_0 at three representative temperatures: $T = 0$, $T = T_s(\theta_0)$, and $T = T_s(\theta_0) + 0.025\epsilon/k_B$. The final densities reached at $T = 0$ do not depend very strongly on θ_0 ; the densest system ($\theta_0 = 120^\circ$) is only $\sim 6\%$

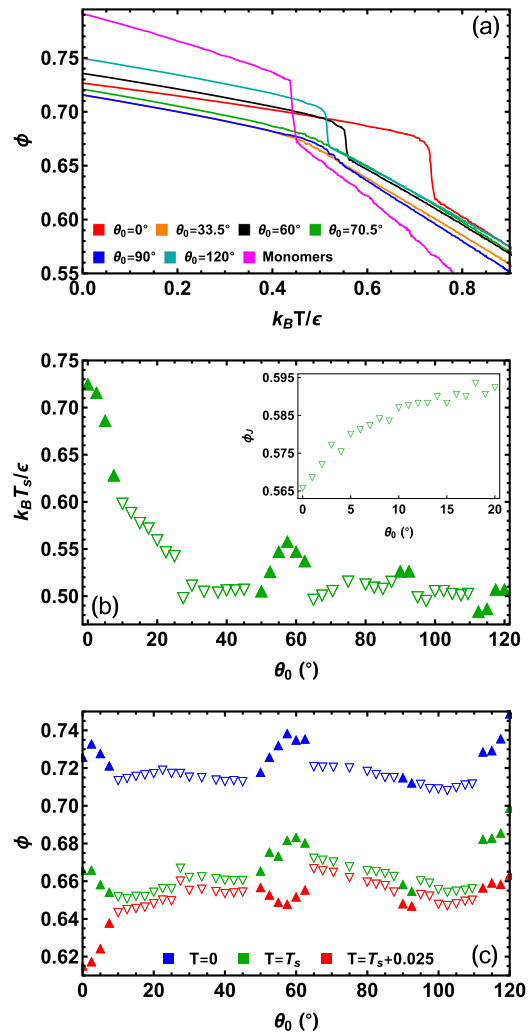


FIG. 3. Basic solidification results for bent-core trimers. Panel (a): Packing fraction $\phi(T)$ for six representative θ_0 and for monomers. Panel (b): Solidification temperatures $T_s(\theta_0)$ for all θ_0 , calculated as described in Sec. II A. The inset compares these to athermal bent-core trimers' $\phi_I(\theta_0)$ for $\theta_0 \leq 20^\circ$.¹¹ Panel (c): Packing fractions for all θ_0 at three representative temperatures, where the $T_s(\theta_0)$ values are the same as in panel (b). In panels (b) and (c), upward (downward) triangles indicate crystal-formers (glass-formers). For comparison, monomers have $T_s = 0.446\epsilon/k_B$, $\phi(0) = 0.791$, $\phi(T_s) = 0.697$, and $\phi(T_s + 0.025\epsilon/k_B) = 0.663$.³³

more tightly packed than the least-dense system ($\theta_0 = 102.5^\circ$). The broad minimum around $\theta_0 = 102.5^\circ$ is consistent with—and to some extent³⁴ supports—Lewis-Wahnström-like models' choice of $\theta_0 = 105^\circ$ as a bond angle suitable for modeling glassforming trimer-like molecules such as OTP.^{5–9} Similar trends with θ_0 are apparent at $T = T_s$; the θ_0 -dependence of $\phi(0) - \phi(T_s)$ is fairly weak. In contrast, the much stronger θ_0 -dependence of $\phi(T_s) - \phi(T_s + 0.025\epsilon/k_B)$ reflects the trends shown in panel (b), i.e., small- θ_0 trimers crystallize from much-lower-density supercooled liquids than their large- θ_0 counterparts.

B. Microscopic

The wide range of thermal solidification behavior highlighted in Fig. 3 results entirely from changing the bond angle θ_0 , i.e., from changing trimers' shape. This suggests that it can be understood at a microscopic level by applying tools and concepts like those applied to model atomic/colloidal systems in Refs. 22–29.

Figure 4 shows snapshots of $\theta_0 = 70.5^\circ$ and $\theta_0 = 120^\circ$ systems at $T = T_s + 0.025\epsilon/k_B$, T_s , and 0, with monomers color-coded by their CCE norms. The systems appear similar at $T_s + 0.025\epsilon/k_B$, while a few fivefold-symmetric sites are present, most lack any distinguishable order. For the $\theta_0 = 70.5^\circ$ systems, the only obvious changes as T decreases are that more fivefold-symmetric sites appear, as do a very small number of HCP-ordered sites. The behavior of $\theta_0 = 120^\circ$

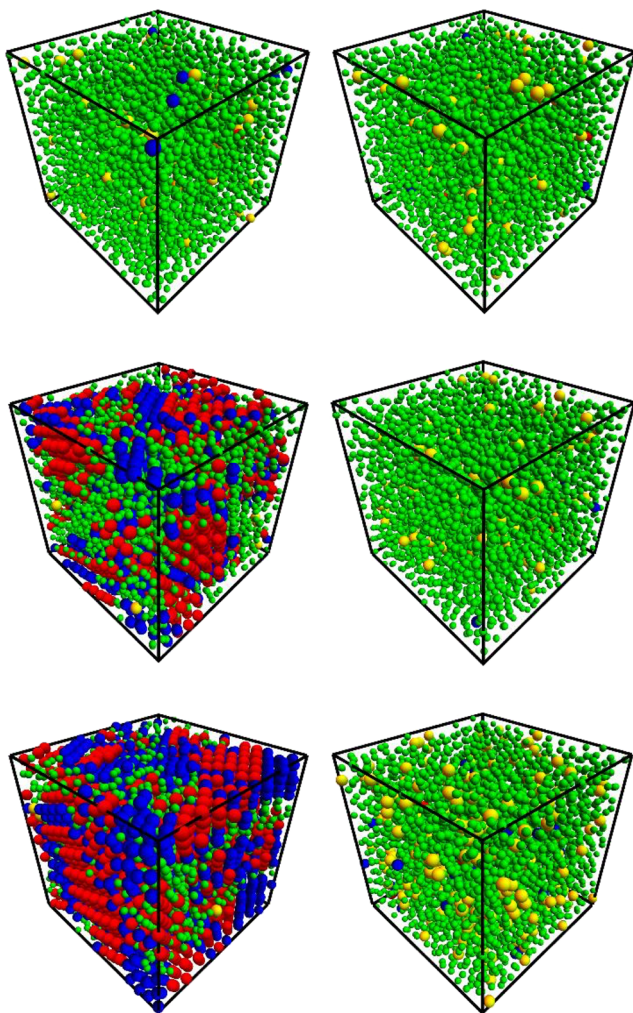


FIG. 4. Snapshots of the best-crystallizing ($\theta_0 = 120^\circ$; left panels) and best-glassforming ($\theta_0 = 70.5^\circ$; right panels) systems at $T = T_s + 0.025\epsilon/k_B$ (top panels), $T = T_s$ (middle panels), and $T = 0$ (bottom panels). Red, blue, yellow, and green indicate monomers classified as FCC, HCP, fivefold-symmetric, and "other," respectively.

trimers is very different. A large degree of mixed FCC/HCP order is present by $T = T_s$, and a relatively well-ordered crystal develops as T decreases further; the $T = 0$ snapshot clearly shows crystalline grains separated by stacking faults and the amorphous interphase. Since these two θ_0 , respectively, have the lowest and highest fraction of close-packed monomers at $T = 0$, we characterize them as the best glass-former and best crystal-former.

We now examine these differences more quantitatively. Figure 5 shows $f_X(T)$ for these systems. Panel (a) illustrates how the crystal-former shows sharp (and typical^{22,23}) upward jumps in both f_{FCC} and f_{HCP} and sharp downward jumps in f_{5f} and $f_{\text{oth}} \equiv 1 - (f_{\text{FCC}} + f_{\text{HCP}} + f_{5f})$ at $T = T_s$, whereas the glass-former shows no such jumps. Intriguingly, the total fraction of locally close-packed monomers $f_{cp} \equiv f_{\text{FCC}} + f_{\text{HCP}}$ is about an order of magnitude higher in the crystal-former at temperatures slightly above T_s than it is in the glass-former, presumably indicating the crystal-forming liquid's greater population of subcritical nuclei. The results from TCC analyses [panel (b)] show analogous trends; the crystal-former shows sharp (and typical^{26,29}) upward jumps in both f_{6A} and f_{9K} and sharp downward jumps in f_{6Z} and f_{9B} at $T = T_s$, whereas the glass-former does not. Remarkably, the formation propensity of mid-size crystalline clusters, e.g., 9K (midsize amorphous clusters, e.g., 9B), is significantly higher (lower) in the crystal-former even at $T \simeq 1.5T_s$.

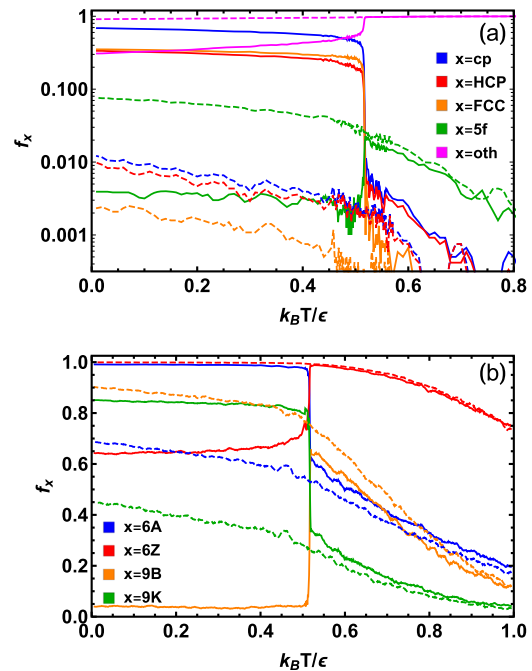


FIG. 5. CCE and TCC results: $f_X(T)$ for selected θ_0 . Solid and dashed curves show the results for the best crystal-former ($\theta_0 = 120^\circ$) and the best glassformer ($\theta_0 = 70.5^\circ$), respectively. To suppress finite-system-size noise, data for $|T - T_s| > 0.02\epsilon/k_B$ are smoothed using moving averages. The negative $\partial f_X/\partial T$ for $T \gtrsim T_s + 0.1\epsilon/k_B$ in panel (b) are driven primarily by changes in ϕ (i.e., by thermal expansion) rather than changes in orientational order.³⁵

These differences between $\theta_0 = 70.5^\circ$ and $\theta_0 = 120^\circ$ systems are consistent with the trends seen in numerous model colloidal systems.^{22–29} Considered in isolation, they are not surprising. What is surprising is that they are so stark despite the fact that both $\theta_0 = 70.5^\circ$ and $\theta_0 = 120^\circ$ trimers can form 3D close-packed crystals.¹¹ We now attempt to understand them further by comparing CCE and TCC results for all θ_0 .

Figure 6 shows the θ_0 -dependence of $f_X(T)$ for $T = 0$, T_s , and $T_s + 0.025\epsilon/k_B$. Panel (a) summarizes the essential features of the bond angle's effect on crystallizability. $f_{cp}(0)$ exhibits four broad maxima centered at $\theta_0 \simeq 0^\circ$, 60° , 90° , and 120° . These four θ_0 all allow formation of both FCC and HCP crystals. $\theta_0 = 0^\circ$, 60° , and

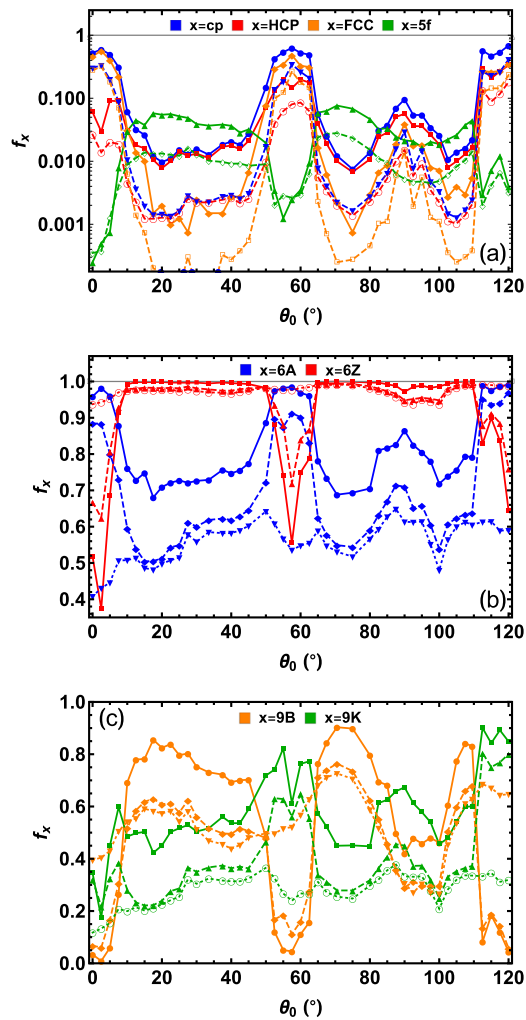


FIG. 6. CCE and TCC results: f_X for all θ_0 at selected T . Panel (a) shows the results for close-packed and fivefold-symmetric structures, while panels (b) and (c) show the results for the 6-particle and 9-particle clusters, respectively, schematically depicted in Fig. 2. In all panels, solid, dashed, and dotted curves show $f_X(\theta_0)$ at $T = 0$, $T = T_s(\theta_0)$, and $T = T_s(\theta_0) + 0.025\epsilon/k_B$, respectively. Note that incommensurability of θ_0 with bulk close-packing does not preclude the formation of small close-packed crystallites.¹¹

120° trimers all have $f_{cp}(0) > 0.5$. $\theta_0 = 90^\circ$ trimers crystallize far less well: their $f_{cp}(0) \simeq 0.1$. A potential explanation for this difference is suggested by the fact that $\theta_0 = 0^\circ$, 60° , and 120° trimers can tile the 2D triangular lattice, whereas $\theta_0 = 90^\circ$ trimers cannot. Specifically, if crystal nuclei preferentially grow by trimers attaching to their triangular ($\{1\ 1\ 1\}$) lattice planes, their growth kinetics will necessarily be slower for $\theta_0 = 90^\circ$ than for $\theta_0 = 0^\circ$, 60° , and 120° .

Figure 6(a) also illustrates a second key difference between crystal-forming and glass-forming systems. Most crystal-formers exhibit comparable f_{FCC} and f_{HCP} for $T \lesssim T_s$. This is not surprising; formation of RHCP-crystalline order is typical for pair interactions ranging from Lennard-Jones to hard-spherical.³⁶ What is surprising is that the formation of FCC (but not HCP) order is strongly suppressed in all glass-forming systems. The reason for this suppression is clear for $\theta_0 = 33.5^\circ$ and 70.5° —these trimers can tile the HCP but not the FCC lattice—and the full $f_{FCC}(T_s)$ dataset suggests that this suppression of FCC relative to HCP ordering extends to θ_0 well away from these special values. This is a nontrivial result because trimers with any $\theta_0 \leq 120^\circ$ ($\theta_0 \leq 60^\circ$) can form close-packed bilayers (trilayers).¹¹

The θ_0 -dependence of the TCC cluster populations at these three characteristic temperatures reinforces the above observations. Figure 6(b) shows three clear maxima [minima] of $f_{6A}(0)$ [$f_{6Z}(0)$] at $\theta_0 \simeq 0^\circ$, 60° , and 120° . These match the trends in f_{cp} shown in panel (a)—sensibly so, because small crystalline clusters like 6A support close-packing while small amorphous clusters like 6Z suppress it.^{25–29} The higher- T results for f_{6A} and f_{6Z} are less conclusive; crystal formers show greater increases in f_{6A} as T approaches T_s from above, but the trends in f_{6Z} are not notably different for crystal-formers vs glass-formers.

Clearer predictive distinctions emerge at the nine-particle level [Fig. 6(c)]. For $60^\circ \lesssim \theta_0 \lesssim 100^\circ$, glass-formers have notably higher f_{9B} at $T = T_s + 0.025\epsilon/k_B$, and the largest f_{9B} for $T \geq T_s$ occurs in $\theta_0 = 70.5^\circ$ systems. Although partial-icosahedral structures like 9B are well-known to suppress crystallization in atomic/colloidal systems,^{25–29,32} few previous studies of molecular liquids have explored how these structures' formation propensity varies with the constituent molecules' shape, and this result would have been difficult to predict at the single-trimer level, especially since $\theta_0 = 70.5^\circ$ trimers can close-pack. Trends in crystalline-cluster populations (e.g., 9K) are less clear, apart from their notably lower $f_X(T \geq T_s)$ for $\theta_0 \lesssim 20^\circ$, which is consistent with these systems' higher T_s and lower $\phi(T_s)$.³⁵

Thus far, our cluster-level analyses have treated all monomers equally and ignored dynamics. This approach is incomplete because we are considering molecular (i.e., trimeric) liquids and because cluster-level dynamics are critical in determining glass-formability.^{27,28} Figure 7 illustrates the additional insights that can be gained at the six-particle level. In panel (a), $f_X^{tri}(T)$ is the fraction of trimers that lie entirely within a cluster of type X. Differences between the best crystal-former and the best glass-former are far more dramatic than those illustrated in Fig. 5(b). Although many monomers in the $\theta_0 = 70.5^\circ$ liquid lie within 6A clusters, very few trimers do. In the $\theta_0 = 120^\circ$ liquid, however, many trimers lie within 6A clusters even at $T = 3T_s/2$. Thermal diffusive motion of these trimers should make the 6A cluster lifetime much shorter in the $\theta_0 = 70.5^\circ$ liquid than it is in the $\theta_0 = 120^\circ$ liquid. Panel (b) confirms this hypothesis: $P_X^s(T)$ is the probability that a given cluster of type X

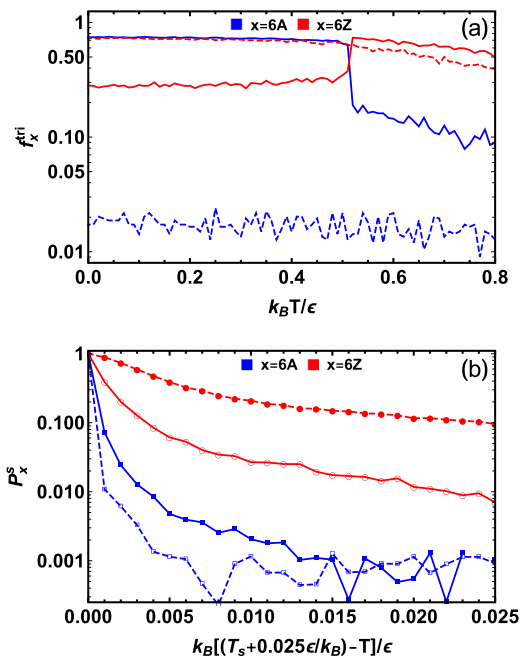


FIG. 7. Comparison of trimer-level ordering and cluster stability in the best crystal-former (solid curves) vs the best glass-former (dashed curves). Panel (a): $f_x^{tri}(T)$. Panel (b): $P_x^s(T)$.

that is present at $T_s + 0.025\epsilon/k_B$ is still present when the temperature has dropped to T . The data show that 6A (6Z) clusters are far more stable in $\theta_0 = 120^\circ$ ($\theta_0 = 70.5^\circ$) liquids in this temperature range. Note that these dramatic differences in cluster stability are present despite the fact that the two systems' T_s are almost identical. While one might argue that they should have been expected because 70.5° is very close to the ideal fivefold-symmetry-promoting bond angle (72°), we emphasize that they occur despite the fact that $\theta_0 = 70.5^\circ$ trimers can close-pack.¹¹

IV. DISCUSSION AND CONCLUSIONS

We examined how thermal solidification of bent-core trimers is influenced by their bond angle θ_0 . Their solidification temperature $T_s(\theta_0)$ is relatively constant for $\theta \gtrsim 20^\circ$, but increases rapidly with decreasing $\theta_0 \lesssim 20^\circ$ owing to the reduction in trimers' effective configurational freedom as they straighten. This decreasing freedom also produces a sharp decrease in athermal bent-core trimers' $\phi_f(\theta_0)$ as $\theta_0 \rightarrow 0^\circ$.¹¹ We therefore conclude that these systems' thermal-solidification (not just glass-formation) and jamming transitions are intimately connected, in a manner consistent with the ideas of Liu and Nagel.³⁷ Similar connections have recently been demonstrated for polymers.^{38,39}

On the other hand, our results also illustrate a fascinating *contrast* between thermal and athermal solidification. In athermal 3D systems, the competition between FCC and HCP ordering suppresses crystallization because it produces random-close-packed amorphous order.^{40,41} In thermal trimer solidification, however, it

seems that the *absence* of this competition suppresses crystallization. It is reasonable to suppose that HCP crystallites have a higher nucleation barrier (ΔG) than those of mixed FCC/HCP order owing to their lower entropy. A higher ΔG for trimers that can form only HCP crystals would make them less likely to crystallize (under cooling at a fixed rate \dot{T}) than the trimers that can form both FCC and HCP order. This is indeed what we observe and is consistent both with Pedersen *et al.*'s finding that Lewis-Wahnstrom-like trimers glass-form more readily than monomeric Lennard-Jones systems primarily because their crystal nucleation barrier is higher^{6–8} and with Russo and Tanaka's conclusion that $\beta\Delta G$ is the key quantity controlling glass-formability.⁴²

We found that bent-core trimers exhibit a wide range of solidification behaviors; some are very good crystal-formers, while others are very good glass-formers. By examining all six of the θ_0 that are commensurable with 3D close-packing, we showed that these differences do not arise from geometric frustration. Instead, our CCE and TCC analyses showed that they arise from θ_0 -dependent differences in trimer liquids' tendencies to form local cluster-level structure that is stable and inhibits crystallization. Factors promoting greater stability of 6Z and other amorphous clusters (6A and other ordered clusters) unambiguously promote glass-formation (crystallization). The difference between the present study and previous studies with comparable findings^{22–29} is that in trimer liquids the relative strength of these factors is determined by the quenched 2- and 3-body constraints (i.e., by the values of R and θ_0) rather than by details of the pairwise interactions or preparation protocol.

One of the principal goals of soft materials science is developing materials with tunable solid morphology. This can be done either by trial-and-error or by developing theories that predict the optimal molecular structure for obtaining a desired morphology and then synthesizing molecules possessing this structure. The latter approach, now commonly known as “molecular engineering,” has attracted great interest in recent years and has been applied to systems ranging from photonic crystals⁴³ to hydrogels.⁴⁴ The results presented in this paper should be a useful contribution to this effort because controlling bond angles in isomeric and near-isomeric small molecules is a molecular-engineering strategy that is often employed by experimentalists.^{3,4,45,46}

ACKNOWLEDGMENTS

This material was based on work supported by the National Science Foundation under Grant No. DMR-1555242. We thank Austin D. Griffith for helpful discussions.

APPENDIX: $|\dot{T}|$ -DEPENDENCE AND GLASSY DYNAMICS

Precisely determining $T_{\text{melt}}(\theta_0)$ would require extensive simulations employing advanced techniques^{6–8} and is beyond our scope. Here, to support our claim (Sec. II A) that $\Delta T(\theta_0)$ is small for our best crystal-formers, we illustrate how $T_s(\theta_0)$ depends on \dot{T} . Figure 8 shows $\phi(T)$ results for $|\dot{T}|$ spanning a factor of 100—from 10 times slower to 10 times higher than that employed above. The $|\dot{T}|$ -dependence is extremely weak for the glass-forming systems ($\theta_0 = 33.5^\circ$ and 70.5°), indicating that their critical crystal

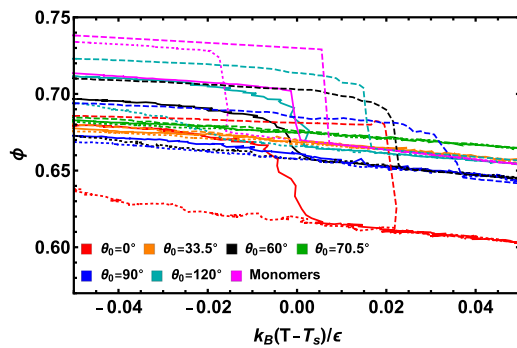


FIG. 8. Cooling-rate dependence of solidification for bent-core trimers. Dotted, solid, and dashed lines show the results for $k_B\tau|\dot{T}|/\epsilon = 10^{-5}$, 10^{-6} , and 10^{-7} , respectively. The results are plotted vs $T - T_s(\theta_0)$, where the $T_s(\theta_0)$ values are those reported in Fig. 3, i.e., the values of T_s for $k_B\tau|\dot{T}|/\epsilon = 10^{-6}$.

nucleation rates are well below $10^{-7}/\tau$. As expected, the crystal-forming systems exhibit larger (smaller) jumps in $\phi(T)$ at higher (lower) T , and hence higher (lower) T_s , for lower (higher) $|\dot{T}|$. However, these differences in T_s are small, especially for monomers and $\theta_0 = 120^\circ$ trimers.

We asserted that the dramatic increase in $T_s(\theta_0)$ [and decrease in $\phi(\theta_0)$ in athermal systems¹¹] with decreasing $\theta_0 \lesssim 20^\circ$ is caused by the reduction of effective configurational freedom as trimers straighten. This idea could be tested by comparing the decays of the correlation functions

$$\mathcal{R}(t) = \langle \vec{R}_{ee}(t') \cdot \vec{R}_{ee}(t' + t) \rangle \quad (\text{A1})$$

and

$$C(t) = \langle \vec{c}(t') \cdot \vec{c}(t' + t) \rangle, \quad (\text{A2})$$

where \vec{R}_{ee} is a trimers' end-end vector, \vec{c} is the cross product of its bond vectors, and the averages are taken over all trimers and all t' , for various θ_0 at equal values of $T - T_{\text{melt}}(\theta_0)$ and/or $T/T_{\text{melt}}(\theta_0)$. An increasing decoupling of the decay times of $\mathcal{R}(t)$ and $C(t)$ with decreasing $\theta_0 \lesssim 20^\circ$ would directly support our assertion. Since performing this measurement in a rigorous fashion will require a high-precision calculation of $T_{\text{melt}}(\theta_0)$,^{6–8} we leave it as a challenge for future work.

REFERENCES

- J. N. Andrews and A. R. Ubbelohde, "Melting and crystal structure: The melting parameters of some polyphenyls," *Proc. R. Soc. London, Ser. A* **228**, 435 (1955).
- D. J. List, C. Alba, L. E. Busse, and C. A. Angell, "Thermodynamic aspects of the vitrification of toluene, and xylene isomers, and the fragility of liquid hydrocarbons," *J. Chem. Phys.* **92**, 617 (1990).
- C. T. Powell, K. Paeng, Z. Chen, R. Richert, L. Yu, and M. D. Ediger, "Fast crystal growth from organic glasses: Comparison of o-terphenyl with its structural analogs," *J. Phys. Chem. B* **118**, 8203 (2014).
- W. Ping, D. Paraska, R. Baker, P. Harrowell, and C. A. Angell, "Molecular engineering of the glass transition: Glass-forming ability across a homologous series of cyclic stilbenes," *J. Phys. Chem. B* **115**, 4696 (2011).
- C. Jennings, M. Ramsay, T. Hudson, and P. Harrowell, "Packing concave molecules in crystals and amorphous solids: On the connection between shape and local structure," *Mol. Phys.* **113**, 2755 (2015).
- U. R. Pedersen, T. S. Hudson, and P. Harrowell, "Crystallization of the Lewis-Wahnstrom ortho-terphenyl model," *J. Chem. Phys.* **134**, 114501 (2011).
- U. R. Pedersen and P. Harrowell, "Factors contributing to the glass-forming ability of a simulated molecular liquid," *J. Phys. Chem. B* **115**, 14205 (2011).
- U. R. Pedersen, "Glass-forming ability of Lennard-Jones trimers," e-print [arXiv:1907.01792](https://arxiv.org/abs/1907.01792) (2019).
- L. J. Lewis and G. Wahnstrom, "Molecular-dynamics study of supercooled orthoterphenyl," *Phys. Rev. E* **50**, 3865 (1994).
- A. D. Griffith and R. S. Hoy, "Densest versus jammed packings of two-dimensional bent-core trimers," *Phys. Rev. E* **98**, 042910 (2018).
- A. D. Griffith and R. S. Hoy, "Densest versus jammed packings of bent-core trimers," *Phys. Rev. E* **100**, 022903 (2019).
- V. Meenakshisundaram, J.-H. Hung, and D. S. Simmons, "Design rules for glass formation from model molecules designed by a neural-network-biased genetic algorithm," *Soft Matter* (published online).
- N. C. Karayiannis, K. Foteinopoulou, and M. Laso, *J. Chem. Phys.* **130**, 074704 (2009).
- A. Malins, S. R. Williams, J. Eggers, and C. P. Royall, "Identification of structure in condensed matter with the topological cluster classification," *J. Chem. Phys.* **139**, 234506 (2013).
- The other source of frustration is that for Lennard-Jones interactions, the equilibrium nearest-neighbor distance in a zero-pressure zero- T FCC or HCP lattice is $\sim 0.97\sigma$ ¹⁶ rather than σ owing to $U_L(r)$'s long-range attractive tail. The effects of this discrepancy are negligible at $T \approx T_s$ because the width of the first peak in the pair correlation function $g(r)$ is considerably larger than 0.03σ .
- P. Schwerdtfeger, N. Gaston, R. P. Krawczyk, R. Tonner, and G. E. Moyano, "Extension of the Lennard-Jones potential: Theoretical investigations into rare-gas clusters and crystal lattices of He, Ne, Ar, and Kr using many-body interaction expansions," *Phys. Rev. B* **73**, 064112 (2006).
- H. Kamberaj, R. J. Low, and M. P. Neal, "Time reversible and symplectic integrators for molecular dynamics simulations of rigid molecules," *J. Chem. Phys.* **122**, 224114 (2005).
- S. Plimpton, "Fast parallel algorithms for short-range molecular-dynamics," *J. Comput. Phys.* **117**, 1 (1995).
- The packing fraction in systems interacting via Lennard-Jones or other soft potentials is not very well defined. Typically, one defines an effective hard-sphere radius σ_{eff} and then approximate $\phi \approx \pi h \rho \sigma_{\text{eff}}^3 / 6$. Two definitions of σ_{eff} that could be appropriate for our systems are the zero- P zero- T FCC nearest-neighbor distances are given in Ref. 16, and a temperature-dependent $\sigma_{\text{eff}}(T)$ is defined using the Noro-Frenkel procedure.²⁰ Since the first option makes little physical sense at high T and the second option makes little physical sense at low T , we elect to employ the approximation $\phi = \pi \rho \sigma^3 / 6$.
- M. G. Noro and D. Frenkel, "Extended corresponding-states behavior for particles with variable range attractions," *J. Chem. Phys.* **113**, 2941 (2000).
- A. L. Greer, "Metallic glasses," *Science* **267**, 1947 (1995).
- N. Ch. Karayiannis, R. Malshe, J. J. de Pablo, and M. Laso, "Fivefold symmetry as an inhibitor to hard-sphere crystallization," *Phys. Rev. E* **83**, 061505 (2011).
- N. Ch. Karayiannis, R. Malshe, M. Kröger, J. J. de Pablo, and M. Laso, "Evolution of fivefold local symmetry during crystal nucleation and growth in dense hard-sphere packings," *Soft Matter* **8**, 844 (2012).
- N. C. Karayiannis, K. Foteinopoulou, and M. Laso, "Spontaneous crystallization in athermal polymer packings," *Int. J. Mol. Sci.* **14**, 332 (2013).
- J. Taffs, A. Malins, S. R. Williams, and C. P. Royall, "The effect of attractions on the local structure of liquids and colloidal fluids," *J. Chem. Phys.* **133**, 244901 (2010).
- J. Taffs, S. R. Williams, H. Tanaka, and C. P. Royall, "Structure and kinetics in the freezing of nearly hard spheres," *Soft Matter* **9**, 297 (2013).
- A. Malins, J. Eggers, H. Tanaka, and C. P. Royall, "Lifetimes and lengthscales of structural motifs in a model glassformer," *Faraday Discuss.* **167**, 405 (2013).
- A. Malins, J. Eggers, C. P. Royall, S. R. Williams, and H. Tanaka, "Identification of long-lived clusters and their link to slow dynamics in a model glass former," *J. Chem. Phys.* **138**, 12A535 (2013).
- C. P. Royall and S. R. Williams, "The role of local structure in dynamical arrest," *Phys. Rep.* **560**, 1 (2015).

- ³⁰G. Meng, N. Arkus, M. P. Brenner, and V. N. Manoharan, “The free-energy landscape of clusters of attractive hard spheres,” *Science* **327**, 560 (2010).
- ³¹A. V. Anikeenko and N. N. Medvedev, “Polytetrahedral nature of the dense disordered packings of hard spheres,” *Phys. Rev. Lett.* **98**, 235504 (2007).
- ³²F. C. Frank, “Supercooling of liquids,” *Proc. R. Soc. London, Ser. A* **215**, 43 (1952).
- ³³Systems with Lennard-Jones pair interactions can reach ϕ values above the hard-sphere close-packing density ($\phi_{cp} = \pi/\sqrt{18} \simeq 0.7405$) because the long-range attractive tail of $U_{LJ}(r)$ makes the equilibrium nearest-neighbor distance $r_{nn} < \sigma$ in close-packed crystals.¹⁶
- ³⁴Direct comparison of our results to those for LW-like models is not straightforward because the LW model has $R = 2^{1/6}$.
- ³⁵TCC clusters include a core monomer and other monomers in its first coordination shell; the latter are identified using a modified Voronoi method.¹⁴ The decrease in cluster populations as T increases and ρ decreases appears to be driven primarily by the concomitant decrease in coordination number.
- ³⁶S. Torquato, “Perspective: Basic understanding of condensed phases of matter via packing models,” *J. Chem. Phys.* **149**, 020901 (2018).
- ³⁷A. J. Liu and S. R. Nagel, “Nonlinear dynamics—Jamming is not just cool any more,” *Nature* **396**, 21 (1998).
- ³⁸R. S. Hoy, “Jamming of semiflexible polymers,” *Phys. Rev. Lett.* **118**, 068002 (2017).
- ³⁹C. O. Plaza-Rivera, H. T. Nguyen, and R. S. Hoy, “Isostaticity and the solidification of semiflexible polymer melts,” *Soft Matter* **13**, 7948 (2017).
- ⁴⁰B. D. Lubachevsky, F. H. Stillinger, and E. N. Pinson, “Disks vs spheres: Contrasting properties of random packings,” *J. Stat. Phys.* **64**, 501 (1991).
- ⁴¹S. Torquato, T. M. Truskett, and P. G. Debenedetti, “Is random close packing of spheres well defined?,” *Phys. Rev. Lett.* **84**, 2064 (2000).
- ⁴²J. Russo, F. Romano, and H. Tanaka, “Glass forming ability in systems with competing orderings,” *Phys. Rev. X* **8**, 021040 (2018).
- ⁴³W. P. Lustig, S. Mukherjee, N. D. Rudd, A. V. Desai, J. Li, and S. K. Ghosh, “Metal-organic frameworks: Functional luminescent and photonic materials for sensing applications,” *Chem. Soc. Rev.* **46**, 3242 (2017).
- ⁴⁴T. Jungst, W. Smolan, K. Schacht, T. Scheibel, and J. Groll, “Strategies and molecular design criteria for 3D printable hydrogels,” *Chem. Rev.* **116**, 1496 (2015).
- ⁴⁵T. Liu *et al.*, “Birefringent stable glass with predominantly isotropic molecular orientation,” *Phys. Rev. Lett.* **119**, 095502 (2017).
- ⁴⁶R. Teerakapibal, C. Huang, A. Gujral, M. D. Ediger, and L. Yu, “Organic glasses with tunable crystalline order,” *Phys. Rev. Lett.* **120**, 055502 (2018).